Chemistry Europe
European Chemical Societies Publishing

WILEY VCH

Excellence in Chemistry Research

Announcing our new flagship journal

- Gold Open Access
- Publishing charges waived
- Preprints welcome
- Edited by active scientists

Meet the Editors of *ChemistryEurope*

Luisa De Cola
Università degli Studi di Milano Statale, Italy

Ive Hermans
University of Wisconsin-Madison, USA

Ken Tanaka
Tokyo Institute of Technology, Japan

ChemCatChem

Research Article
doi.org/10.1002/cctc.202201622

Chemistry Europe
European Chemical Societies Publishing

www.chemcatchem.org

Special Collection

Design of Multicationic Copper-Bearing Layered Double Hydroxides for Catalytic Application in Biorefinery

Iqra Zubair Awan,[a, b, c] Phuoc Hoang Ho,[a, d] Giada Beltrami,[e] Olinda Gimello,[a] Thomas Cacciaguerra,[a] Pierrick Gaudin,[a] Nathalie Tanchoux,[a] Stefania Albonetti,[b] Annalisa Martucci,[e] Fabrizio Cavani,[b] Didier Tichit,[a] and Francesco Di Renzo*[a]

Ethanol has been used as a renewable hydrogen-donor in the conversion of a lignin model molecule in subcritical conditions. Noble metal-free porous mixed oxides, obtained by activation of Cu–Ni–Al and Cu–Ni–Fe layered double hydroxide (LDH) precursors, have been used as heterogeneous catalysts for Meerwein-Ponndorf-Verley (MPV) hydrogen transfer and further hydrogenation by ethanol dehydrogenation products. Both the Cu/(Cu + Ni) ratio and the nature of the trivalent cation (Al or Fe) affect the activity of the catalysts, as well as the selectivity towards the different steps of the hydrogenation reactions and the cleavage of lignin-like phenylether bonds. Accounting for the peculiar behaviour of Cu^{2+} and M(III) cations in the synthesis of LDHs, the coprecipitation of the precursors has been monitored by titration experiments. Structural and textural properties of the catalysts are closely related to the composition of the LDH precursors.

Introduction

The growing interest in replacing oil-derived chemicals by bio-based molecules is drawing increased attention on the lignin fraction of lignocellulosic biomass, a poorly exploited renewable source of aromatics. The extraction of valuable lignin-derived chemicals during the fractionation of lignocellulosic biomass was initially addressed in organosolv pulping processes, by the use of appropriate solvents in acid or basic conditions.[1] More recently, organosolv pulping has found a new revival in lignin-first biorefineries, in which heterogeneous catalysis of hydrogenation reactions has been introduced in the biomass fractionation process.[2] The resulting increase of H/C and decrease of O/C ratios contribute to the improved separation of phenolics and open new markets for lignin products.[3] It has been suggested that catalytic hydrogen transfer from hydrogen-donor solvents can replace hydrogenation by H_2 molecules in lignocellulose pulping.[4] This has prompted a renewed interest in heterogeneous catalysts of MPV (Meerwein-Ponndorf-Verley) hydrogen transfer in organosolv pulping, notably by the development of porous copper-bearing mixed oxides obtained from activation of layered double hydroxide (LDH) precursors.[5]

The interest of LDHs as precursor of catalysts mainly depends on the wide variety of cations that can be uniformly distributed in the structure by syntheses in mild precipitation conditions. LDHs are a family of lamellar compounds whose chemical composition is expressed by the general formula $[M^{II}_{1-x}M^{III}_{x}(OH)_2][(A^{n-})_{x/n}.m\ H_2O]$, where M^{II} and M^{III} represent divalent and trivalent cations; A^{n-} stands for the n-valent anion; m is the number of water molecules and x the molar fraction of trivalent cation which for the most stable LDH is between 0.2 and 0.4. Calcination of the precursor LDHs is a versatile method for the preparation of effective mixed oxide catalysts. It is particularly the case for LDHs based on transition metal cations, e.g. Cu^{2+}, Ni^{2+} Co^{2+}, which are effective precursors of catalysts used in an increasing range of industrial processes.[6] A Cu–Zn–Al LDH was the precursor of the low-pressure methanol (LPM) catalyst by ICI, at the basis of the production of methanol since 1965.[7] Catalysts based on Cu–Zn–Al LDH precursors have been extensively used in water gas shift reaction,[8] steam

[a] Dr. I. Z. Awan, Dr. P. H. Ho, Dr. O. Gimello, T. Cacciaguerra, Dr. P. Gaudin, Dr. N. Tanchoux, Dr. D. Tichit, Dr. F. Di Renzo
ICGM
University of Montpellier-CNRS-ENSCM
1919 Route de Mende
34090 Montpellier (France)
E-mail: Francesco.di-renzo@umontpellier.fr
[b] Dr. I. Z. Awan, Prof. S. Albonetti, Prof. F. Cavani
Department of Industrial Chemistry "Toso Montanari"
Alma Mater Studiorum Università di Bologna
Viale Risorgimento, 4
40136 Bologna (Italy)
[c] Dr. I. Z. Awan
Department of Chemistry
Lahore Garrison University
Main Campus, Sector-C, DHA Phase VI
54000 Lahore (Pakistan)
[d] Dr. P. H. Ho
Competence Centre for Catalysis
Chalmers University of Technology
Kemivägen 4
SE.412 96 Gothenburg (Sweden)
[e] G. Beltrami, A. Martucci
Dipartimento di Fisica e Scienze della Terra
Università degli Studi di Ferrara
Via Saragat, 1
44100 Ferrara (Italy)

Supporting information for this article is available on the WWW under https://doi.org/10.1002/cctc.202201622

Special Collection

This publication is part of a Special Collection on "French Conference on Catalysis 2022". Please check the ChemCatChem homepage for more articles in the collection.

reforming and dehydrogenation of alcohols,[9] or phenol hydroxylation.[10]

The importance of the composition and structural features of the LDH precursors, as well as of the activation conditions, on the properties of the derived mixed oxide catalysts has been often stressed.[11] Synthesis and properties of LDHs have been extensively reviewed.[12] Pure LDH phases are easily formed with divalent and trivalent cations in a wide range of cation size and precipitation conditions (pH, temperature, concentration and mode of mixing of solutions…).

Cu-LDH has been often presented as an exception to this easy formation as it was only obtained for long time in the presence of other divalent cations, therefore only as multicationic structures.[12a,13] The specific behaviour of the Cu-LDHs was attributed to Jahn-Teller distortion of the CuO_6 octahedra, preventing the formation of brucite-type layers with a high content of copper.[12b] In many attempts of synthesis, malachite $Cu_2CO_3(OH)_2$ or gerhardtite $Cu_2(NO_3)(OH)_3$ were instead formed, depending on the nature of the precursor salts.[13b,14]

The alleged difficult formation of Cu-LDHs represented an interesting riddle, as such materials exist in nature, as woodwardite, with a quite low divalent/trivalent cation ratio, which allows a dilution of Cu by Al in the brucite-like layer.[15] Indeed, synthetic Cu–Al LDH has been formed at a low divalent/trivalent cation ratio of 2, in a narrow pH range intermediate between the precipitation conditions of oxysalts and $Cu(OH)_2$.[16] The formation of synthetic analogues of woodwardite with low-temperature long-time synthesis and divalent/trivalent cation ratio of 3 has proved more elusive, often bringing to LDH phases contaminated by CuO.[17] Cu–Al LDH presents an orthorhombic symmetry, instead of the usual rhombohedral symmetry of LDH, a difference attributed to the relaxation of the Jahn-Teller distortion of the CuO_6 octahedra in the layers of the structure.[18] Attempts to synthesize Cu–Fe LDH or Cu–Cr LDH resulted in the formation of oxysalts or hydroxides,[13a,19] despite modelisation has suggested Cu–Fe LDH to be a stable phase.[20]

The use of heterogeneous catalysts in biomass processing is often limited by the need for separation of the catalyst from residual solid biomass. This drawback can be overcome using magnetically separable catalysts.[21] The superparamagnetic properties of Ni-bearing ferrites render them suitable materials for pulping treatments,[22] in which the extraction of lignin leaves abundant solid cellulosic matter. Effective catalysts for biomass treatment require both an improved accessibility and a proven catalytic activity.[23] Catalysts derived from Ni-bearing LDHs are used for steam reforming of hydrocarbons and have featured a high CO_2 selectivity in methane dry reforming.[24] They have been proposed for reactions of oxygenate condensation, like the synthesis of methyl vinyl ketone from acetone.[25] The redox properties of LDH-derived nickel catalysts are exploited in oxidative water remediation treatments,[26] hydrogenation of nitriles or alkynes,[27] and hydroprocessing of heavy oils.[28] Recently, they have been proposed in the catalytic pyrolysis of heavy oils. It can also be remarked that Ni–Fe LDH found extensive applications as electrocatalytic material.[29]

Considering the specific properties provided by Cu and Ni, in the present work, mixed oxides in the Cu–Ni–Fe and Cu–Ni–Al systems, designed for magnetic separation of hydrogen-transfer catalysts, have been prepared from LDH precursors and tested in catalytic hydrogen transfer reactions on a model molecule representative of the main functional groups of lignin. Ethanol, a solvent obtained from renewable resources, has been used as a hydrogen donor in subcritical conditions. The reported difficulties in the formation of Cu-LDH have motivated a preliminary titration study of the synthesis of Cu–Al and Cu–Fe LDH.

Results and Discussion

Monitoring LDH formation

The objective of the work is to design NiCuAl and NiCuFe LDHs as efficient precursors of catalysts for hydrogen transfer valorisation of lignin model molecules. Several previous works have shown that the pH titration curves of the mixed cation solutions are powerful tools for a comprehensive analysis of the LDHs formation.[30] This approach is particularly relevant regarding copper-based LDHs emphasizing the specific behaviour of this divalent cation in such materials. The pH titration curves of multicationic solutions (Cu–Ni–Al and Cu–Ni–Fe) cannot be easily exploited but those of the dicationic solutions containing Ni or Cu as divalent cation and Al or Fe as trivalent cation (Ni–Al, Ni–Fe, Cu–Al and Cu–Fe) are able to provide useful information. The pH titration curves of the mixed Ni–Al and Ni–Fe solutions have been previously reported and discussed,[30a,31] contrary to those of the Cu–Al and Cu–Fe mixed solutions. These latter ones will be studied in the present work.

The number of moles of OH^- consumed per moles of Cu and Al (or Fe) expressed as R ($R = n\ OH^-/(n\ Cu^{2+} + n\ M^{3+})$) is plotted in Figure 1. The obtained curves

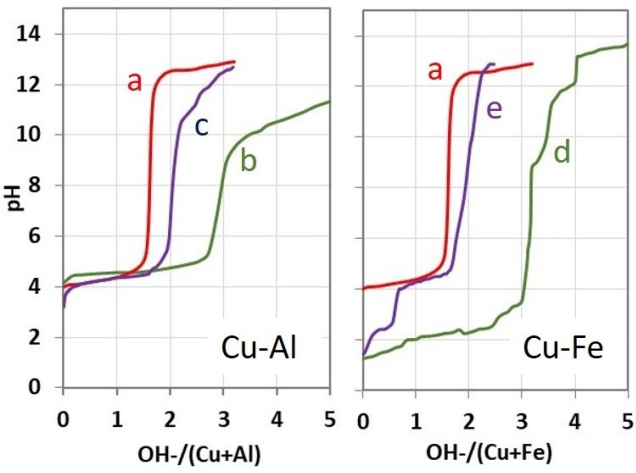

Figure 1. Titration curves in the systems Cu–Al and Cu–Fe: Cu^{2+} (a), Al^{3+} (b), mixed Cu^{2+} and Al^{3+} (c), Fe^{3+} (d) and mixed Cu^{2+} and Fe^{3+} (e). The similar pH of precipitation of Cu^{2+} and Al^{3+} favours the formation of mixed phases.

correspond to the titration of mixed $Cu(NO_3)_2{\cdot}3H_2O$ (0.375 M) and $Al(NO_3)_3{\cdot}9H_2O$ or $Fe(NO_3)_3{\cdot}9H_2O$ (0.125 M) salt solution by NaOH (2 M) at room temperature. Those of each single Cu^{2+}, Al^{3+} and Fe^{3+} cation are also reported for sake of comparison.

The titration curve of the aluminium solution (Figure 1, curve b) exhibits a slight increase up to a quasi-plateau near pH = 4.5 which is extended up to R = 2.7. This evolution corresponds to the progressive hydrolysis and polymerization of Al^{3+} where OH^- reacts first with the hexahydrated $Al(H_2O)_6^{3+}$ species at low pH leading to aluminium aquo hydroxo complexes intermediates such as $Al_2(OH)_4^{2+}$ and $Al_5(OH)_{13}^{2+}$ further polymerizing into larger species such as $Al_{13}O_4(OH)_{24}^{7+}$ and $Al_{30}(OH)_{58}^{32+}$. A steeper increase is observed between R = 2.7 (pH = 4.5) and R = 3 (pH = 9) showing that the polymerization of the species occurs slowly. At pH = 9 a sol gel $Al(OH)_3$ is formed corresponding generally to an amorphous pseudo-boehmite. The slight increase above pH = 9 is assigned to the dissolution of $Al(OH)_3$ to form $Al(OH)_4^-$ species.[32]

The titration curve of the blue copper solution (Figure 1, curve a) with initial pH = 3.6, shows a smooth increase extending until pH = 4.6 at R = 1.5 corresponding to the formation of copper hydroxynitrate $Cu(OH)_{1,5}(NO_3^-)_{0,5}$. An abrupt increase is then observed until R = 2 where a green precipitate corresponds to a mixture of $Cu(OH)_2$ and $Cu(OH)_{1,5}(NO_3)_{0,5}$. At R = 2.3 (pH = 12.5), the suspension becomes a clear green solution and the precipitate is identified as $Cu(OH)_2$ by XRD.

Titration of the deep turquoise blue mixed solution of copper and aluminium nitrates (Cu/Al = 3) (Figure 1, curve c) shows a rapid increase of pH from 3.2 to 4 when the first drops of NaOH are added. An almost horizontal plateau is then observed until R = 2.5. The pH values of this plateau which increase slightly from 4 to 4.6 are higher than those of precipitation of the single aluminium cation until R = 1 and then practically merged with the precipitation of single copper cation between R = 1 and 1.5. Such behaviour is consistent with the independent sequential mechanism of precipitation of the trivalent and then the divalent cation described in the literature for the formation of LDH.[30a] The abrupt increase at about R = 2.8 with an equivalent point at pH = 8 corresponds to the coprecipitation of Cu/Al LDH as confirmed by XRD and previous reports.[33]

The pH titration curve of the yellow iron nitrate solution (Figure 1, curve d), with initial pH = 1.3, shows a slow increase to R = 0.75 (pH = 2) followed by a pseudo-plateau whose medium pH is around 2.5 which is extended until R = 3 with formation of a red precipitate. The value R = 3 at the end of the plateau well corresponds to the precipitation of a goethite phase, FeOOH.[31] One can note that FeOOH is formed in presence of NO_3^- anions while previous works have reported different behaviour in presence of Cl^- and SO_4^{2-} anions where akaganeite ($Fe^{III}O(OH,Cl)$) and schwertmannite ($(Fe^{III}O(OH,SO_4)$) phase were formed, respectively.[30e,31] NO_3^- is probably less able to substitute structural hydroxyls or to be incorporated in the tunnels. The iron hydroxide species is totally precipitated at around pH = 8.

Blending blue Cu nitrate (pH 3.6) and yellow Fe nitrate (pH 1.3) solutions gives a deep green mixed solution with pH = 1.3. The curve (Figure 1, curve e) then increases until reaching a first plateau at pH = 2.5 where the solution becomes black. It corresponds to the precipitation of the ferric ions in presence of an excess of Cu^{2+} in the solution. A pH increase is observed from R = 0.6 to reach a second plateau around pH = 4, where the suspension turns brown. The plateau extends up to R = 1.8 (pH = 4.5) and is close to that observed for Cu^{2+} alone, confirming the sequential precipitation of the divalent and trivalent cations of the mixed Cu–Fe solution.

The XRD pattern of the dried precipitate at R = 1.5 corresponds to $Cu_2NO_3(OH)_3$ phase (Figure 2). The pH increases from 4.5 at the end of the plateau to 12.5 at R = 2.5 where the suspension becomes green. The XRD patterns of the dried precipitates during this step reveal the presence of a mixture of $Cu_2NO_3(OH)_3$ and $Cu(OH)_2$ at R = 2 (pH = 9) and of $Cu(OH)_2$ alone at R = 2.5 (pH = 13) (Figure 2). EDX analysis shows that iron is always present in these precipitates and that the Cu/Fe molar ratio increases from 1.6 to 3.3 when going from R = 1.5 to 2.5 due to progressive dissolution of the iron phase. The presence of iron is responsible for the amorphous phase clearly identified by the broad peak centred around 30° in the XRD patterns of the precipitates obtained at R = 2 and 2.5 (Figure 2).

It is noteworthy that the value R = 2.25 at the end of the titration (pH = 13) well corresponds to the precipitation of $Cu(OH)_2$ and $Fe(OH)_3$ with $Fe^{3+}/(Cu^{2+}+Fe^{3+}) = 0.25$ in the synthesis solution.

The pH titration curves of the mixed Cu–Al and Cu–Fe cation solutions and the characterizations by XRD and EDX analyses of the precipitates at various stages of the titration reveal two different behaviours. The main feature is that a CuAl-LDH phase is formed, which precipitated at pH = 8, whereas an LDH phase is not formed in the presence of iron as trivalent cation. Instead, a mixture of $Cu(OH)_2$ and amorphous iron phase is obtained at the end of the coprecipitation (pH = 13). These behaviours probably account for the different reactivity and morphology of the aluminium and iron hydroxide phases formed at the early stage of the process. The pseudo-boehmite $Al(OH)_3$ is a lamellar structure and Cu^{2+} adsorbed on the surface

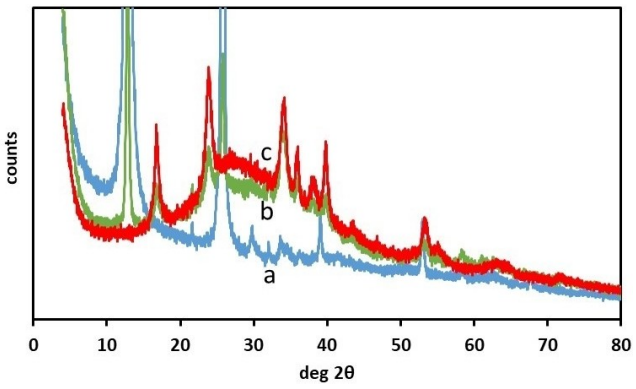

Figure 2. XRD patterns of the dried Cu/Fe precipitates obtained at different alkalinity ratios $OH^-/(Cu+Fe)$: R = 1.5 (a), 2 (b) and 2.5 (c).

at low pH values is progressively inserted in the structure by dissolution-precipitation as the pH increases as previously reported for the Mg–Al system.[34] The initially formed iron hydroxide species is a bulk material and its dissolution rate is probably lower than the precipitation rate of $Cu_2NO_3(OH)_3$ at high nitrate concentration and acid pH. This copper hydroxynitrate phase is thus likely formed in presence of a low amount of dissolved Fe^{3+} in solution.

Phase characterization of as-prepared precursors

The XRD patterns of the Cu–Ni–Al and Cu–Ni–Fe samples with $(Cu+Ni)/M^{III}=3$ (M^{III} = Al or Fe) and $0 \leq Cu/(Cu+Ni) \leq 1$ coprecipitated at pH = 10 and aged at 80 °C are shown in Figure 3.

In the Cu–Ni–Al system, all samples exhibit the characteristic pattern of a well-crystallized LDH phase with 003 and 006 peaks in the 2θ range below 25°, and *0kl* peaks between 30 and 50°. The cell parameter *c* calculated from the d_{003} basal spacing ($c = 3 \times d_{003}$) assuming a rhombohedral symmetry decreases slightly from 23.047 Å for NiAl-LDH to 22.540 Å for CuNiAl-LDH with Cu/(Cu + Ni) = 0.9 (Table 1). The lattice c values depend on the nature of the anion, the average charge of the layers and the amount of interstitial water molecules. Nevertheless, the obtained *c* values are consistent with the intercalation of carbonate anions provided by Na_2CO_3 during synthesis. Besides, it can be assumed that the decrease of the c parameter accounts for an increase in the layer charge of the LDH, well consistent with the formation of additional CuO tenorite phase, detected since Cu/(Cu + Ni) = 0.5 and increasing with the Cu content. These behaviours confirm the easy formation of pure NiAl-LDH with Ni/Al = 3 and, on the contrary, the difficulty to achieve synthesis of rhombohedral CuAl-LDH with high Cu/Al ratio, due to the distortion of the layer structure assigned to Jahn-Teller effect previously reported.[12a] Therefore, a significant amount of copper segregates as CuO phase.

It is noteworthy that the crystallinity in the c direction increases at high Cu/(Cu + Ni) ratio, as shown by the decrease of the full width at half maximum (FWHM) of the 001 peaks (Table 1). Concurrently, the 110 and 113 peaks at around 63° 2θ progressively vanish being no more detected in high-copper CuAl-LDH. This accounts for a regular improvement in stacking of the layers when going from NiAl-LDH to CuAl-LDH and can be related to a concurrent increase in the layer charge.

The lattice parameter *a* calculated from the position of the 110 peak ($a = 2 \times d_{110}$) of the NiCuAl-LDH phases with cationic composition similar to the synthesis solution should slightly decrease when Cu/(Cu + Ni) increases according to the smaller ionic size of Cu^{2+} (0.69 Å) than Ni^{2+} (0.72 Å). Unlike this expected result, a slight increase from 3.040 to 3.050 Å of the *a* parameter is observed when Cu/(Cu + Ni) increases from 0 to 0.5 (Table 1). On the other hand, formation of copper-free phases, due to segregation of copper into CuO phase, should lead to pure NiFe-LDHs with decreasing Ni/Al molar ratios and then contribute to the decrease of the *a* parameter. This behaviour and the observed segregation of CuO since Cu/(Cu + Ni) = 0.5 confirms that the cationic content of the LDH layers does not correspond to that of the solution. Although the exact composition can hardly be established based on the XRD data only, one can suggest that true tricationic NiCuAl-LDH are formed because it is well-known that insertion of copper in the brucite-like layers is facilitated in presence of another divalent cation.[12a]

At higher Cu content, in Cu07Ni68Al25, the diffraction peaks related to the *a* parameter of the rhombohedral structure disappear, whereas the peak multiple of interlayer module becomes narrower (Table 1) and a weak diffraction at 32.75° could be attributed to monoclinic LDH.[18] Ni-free Cu75Al25 presents a single monoclinic phase, with $a = 15.235$ Å, $b = 2.919$ Å, $c = 5.734$, $\beta = 99.99°$ and a very narrow (0.32°) peak at 11.8°.

In the Cu–Ni–Fe system, a LDH phase is detected in all samples with $0 \leq Cu/(Cu+Ni) \leq 0.5$. CuO, tenorite, is also present when $Cu/(Cu+Ni) \geq 0.1$ and is the only phase detected when $Cu/(Cu+Ni) > 0.5$ (Figure 3B). A pure NiFe-LDH whose XRD pattern has a similar shape to that of NiAl-LDH, although less crystallized, is obtained. It is noteworthy that all the Fe-bearing samples are less crystallized than the corresponding Al-bearing ones. It can be underlined that the intensity ratio between the 110 and 00*l* peaks of the LDH phases in the Cu–Ni–Fe system is higher than that in the Cu–Ni–Al system indicating an increase of crystallinity in the (*a*, *b*) direction at the expense of the *c* direction. The main difference with the Cu–Ni–Al system is that, for higher copper content ($Cu/(Cu+Ni) \geq 0.9$), any LDH phase is formed, i.e. pure CuFe-LDH cannot be obtained. The XRD patterns show formation of an amorphous phase with broad maxima around 35 and 60 °2θ.

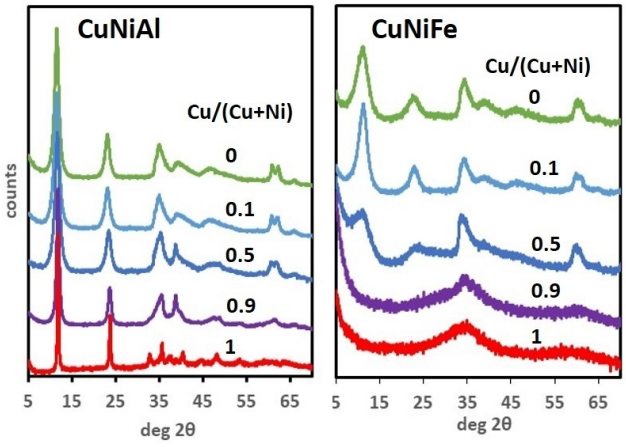

Figure 3. XRD patterns of CuNiAl and CuNiFe samples precipitated at 30 °C and aged at 80 °C. Cu/(Cu + Ni) ratios 0), 0.1, 0.5, 0.9, 1.

Table 1. Cell parameters and peak width of rhombohedral LDH.

Cu/(Cu + Ni)	*c* [Å]		*a* [Å]		FWHM(003)/°2θ	
	CuNiAl	CuNiFe	CuNiAl	CuNiFe	CuNiAl	CuNiFe
0	23.047	22.571	3.040	3.084	1.18	2.9
0.1	23.042	23.300	3.046	3.088	1.25	2.3
0.5	22.755	23.401	3.050	3.097	1.20	3.9
0.9	22.540	n.a.	n.a.	n.a.	0.60	n.a.

This is in accordance with the results of titration experiments. Indeed, the Cu–Fe mixed solution gives rise to the precipitation of CuO and an amorphous iron-rich phase.

The lattice parameter *a* of the Fe-LDH phases are higher than those observed for the Al-bearing LDHs, in agreement with the higher ionic size of Fe^{3+} (0.64 Å) than Al^{3+} (0.50 Å) (Table 1). The evolution of the lattice cell parameter *a* of the Fe-bearing LDHs shows a similar tendency to the previous Al-based LDHs. It indeed increases from 3.084 to 3.097 Å when Cu/(Cu + Ni) increases from 0 to 0.5, unlike the expected behaviour assuming that Cu^{2+} is substituting Ni^{2+} in the amount corresponding to the synthesis solution or that Cu-free samples are formed. This suggests that tricationic CuNiFe-LDHs are formed in the Cu/(Cu + Ni) range from 0.1 to 0.5. Nevertheless, copper must be introduced in limited amounts because pure CuFe-LDH cannot be formed and CuO is largely segregated. Therefore, one can assume that multicationic CuNiFe-LDH phases have lower Cu content than the corresponding CuNiAl-LDHs.

In summary, the characterization by XRD evidenced a different behaviour of the as-prepared samples obtained in the Cu–Ni–Al and Cu–Ni–Fe systems. In the former system, a LDH phase is present in the whole composition range with the CuO phase in addition to the rhombohedral LDH since Cu/(Cu + Ni) = 0.5. In the absence of Ni, pure monoclinic CuAl-LDH is obtained. In the Cu–Ni–Fe system, the rhombohedral LDH phase is only present when Cu/(Cu + Ni) ≤ 0.5 and CuFe-LDH is not formed. Moreover, the nature and content of the obtained phases suggest the formation of copper-richest CuNiAl-LDHs than CuNiFe-LDHs.

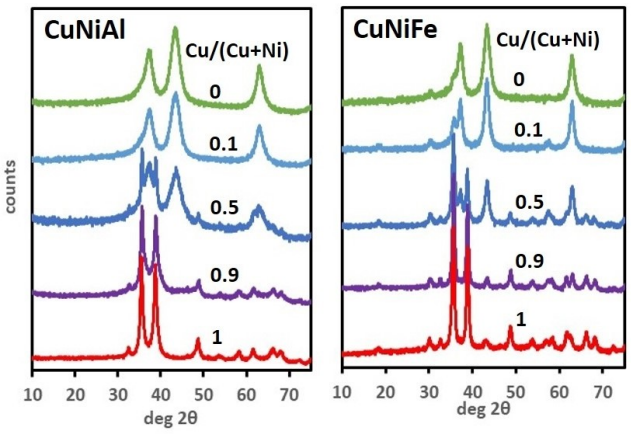

Figure 4. XRD patterns of CuNiAl and CuNiFe catalysts calcined at 600 °C. Cu/(Cu + Ni) ratios 0), 0.1, 0.5, 0.9, 1.

Table 2. Phase ratios, spinel lattice parameter and Scherrer crystallite sizes of catalysts calcined at 600 °C.

	phase [%] (w/w)			*a* [Å]	crystallite size [nm]		
	NiO	spinel	CuO	spinel	NiO	spinel	CuO
Ni75Al25	100.0				3.4		
Cu07Ni68Al25	100.0				3.4		
Cu38Ni37Al25	82.4		17.6		3.1		14.0
Cu68Ni07Al25			100.0				8.4
Cu75Al25			100.0				8.4
Ni75Fe25	84.5	15.5		8.319	10.7	11.8	
Cu07Ni68Fe25	80.0	20.0		8.333	17.1	13.7	
Cu38Ni37Fe25	41.0	27.7	31.3	8.318	16.4	11.8	21.1
Cu68Ni07Fe25	12.0	26.9	61.1	8.339	10.7	9.1	15.6
Cu75Fe25		22.2	77.8	8.424		10.0	17.5

Phase characterization of activated catalysts

The XRD patterns of the catalysts obtained by calcination of the precursors at 600 °C for 6 h under air flow are shown in Figure 4 and the crystalline phase ratios determined by the Rietveld method are reported in Table 2.

The nature and ratio of the crystalline phases as function of the composition differ notably in the two Cu–Ni–M(III) systems with different trivalent elements. The main difference is the presence of a Fe-bearing spinel phase in the CuNiFe system, while no Al-bearing phase is observed in any sample of the CuNiAl series. This clearly indicates the persistence at 600 °C of the amorphous material formed by thermal dehydration of the Al-bearing LDH, in agreement with literature data reporting spinel formation at temperatures beyond 800 °C.[13b,35] The peculiar stability of the amorphous alumina matrix is also confirmed by the retention of Cu and Ni, witnessed by the phase ratios in the mixed samples.

In the Cu–Ni–Al system only one NiO or CuO crystalline phase is present in the two samples containing the largest amounts of nickel (Cu/(Cu + Ni) = 0 and 0.1) and copper (Cu/(Cu + Ni) = 0.9 and 1), respectively. The presence of a single NiO phase in presence of low copper content (Cu/(Cu + Ni) = 0.1) is in accordance with previous reports. Jobbagy et al. indeed found single-phase NiO in $Ni_{1-x}Cu_x(OH)_2$ mixed hydroxides with $x \leq 0.33$ calcined at 400 °C and Rives et al. did not find CuO peaks when the Cu content was not much higher than that of nickel in CuNiAl-LDHs calcined at 500 °C.[36]

The sample Cu38Ni37Al25 presents NiO and CuO crystalline phases in a ratio of 82/18, far from the Cu/Ni ratio of 1/1 in the solid. This confirms that the segregation of the discrete CuO phase is delayed in the presence of NiO until relatively high copper concentration. This clearly suggests a stronger retention of Cu^{2+} than Ni^{2+} in the amorphous alumina material formed by the decomposition of the LDH.

In comparison with the Cu–Ni–Al system, the Cu–Ni–Fe system is characterized by the presence of spinel ferrite phases, whose formation occurs at lower temperature than that generally observed for spinel aluminate. The lattice parameter of the ferrite phase increases with the Cu content from 8.32 Å in Ni75Fe25 to 8.42 Å in Cu75Fe25, in fair agreement with the 8.325 Å literature value for $NiFe_2O_4$ and 8.416 Å for $CuFe_2O_4$.[37]

The NiO and CuO particles exhibit higher mean crystallite sizes in the Cu–Ni–Fe than in the Cu–Ni–Al system. This accounts for the inhibition of the growth of M(II)O oxides by the matrix of amorphous alumina. This represent a further difference with the Cu–Ni–Fe system, where formation of a separate ferrite phase decreases the interaction with the crystallites of divalent oxide.

Textural characterization of catalysts

The N_2 sorption isotherms of the samples calcined at 600 °C are reported in Figure 5 and their textural data in Table 3. The isotherms are type IV, corresponding to mesoporous materials, an important factor for any biorefinery application.[38] The pore diameter for the Ni-richest samples is about 12 and 16 nm for, respectively, the NiAl and NiFe samples. The maximum pore volume in each series is observed for sample with Cu/(Cu + Ni) = 0.1: 0.54 $cm^3 g^{-1}$ for CuNiAl and 0.51 $cm^3 g^{-1}$ for CuNiFe. At the increase of the Cu content, pore volume decreases and pore size increases. The Cu-richest samples present a pore volume near 0.16 $cm^3 g^{-1}$. However, this value has a limited significance, as their isotherms present a limited hysteresis and the mesopore size approaches 50 nm, the conventional borderline between mesoporosity and macroporosity, where adsorption on external surface prevails on condensation in mesopores. The trends of pore volume and size suggest that mesoporosity is largely connected to the presence of small NiO nanocrystals.

Al-bearing samples present a nearly twofold larger surface area than their corresponding Fe-bearing samples, with values in the range 178–44 $m^2 g^{-1}$ and 99–30 $m^2 g^{-1}$, respectively. The difference between the two series could be correlated to the distinct size of the crystallites of the main phases. As indicated in section 3.3, crystallites of both NiO and CuO are smaller in Cu–Ni–Al than in Cu–Ni–Fe series. (Table 2). However, it has to be remarked that the Al-bearing samples contain a significant fraction of amorphous alumina, which contributes to the surface area probably more than the iron-bearing spinels. On the other side, in both series of samples there is a clear tendency toward a decrease of surface area with the increase of copper content. This behaviour is largely due to the increase of the fraction of larger-crystallite CuO at the expenses of smaller-crystallite NiO, albeit such an effect does not completely explain the variations of surface area and the evolution of amorphous material can also play a role.

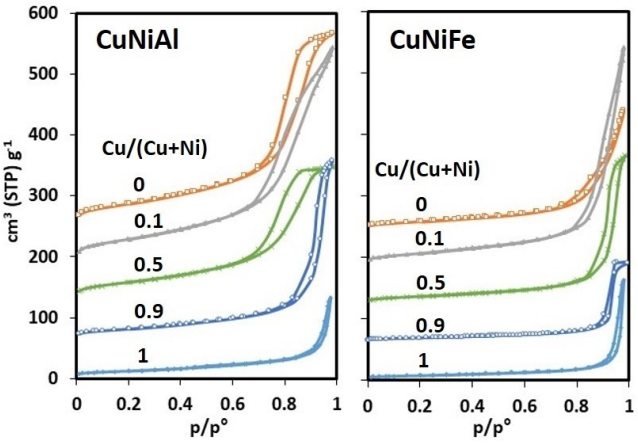

Figure 5. N_2 sorption isotherms of CuNiAl and CuNiFe samples calcined at 600 °C. Cu/(Cu + Ni) ratios 0, 0.1, 0.5, 0.9, 1. The isotherms are shifted by 60 $cm^3 g^{-1}$ for sake of clarity.

Table 3. Surface area, pore volume and average mesopore size of the catalysts.

	Surface area [$m^2 g^{-1}$]	Pore volume [$cm^3 g^{-1}$]	Pore diameter [nm]
Ni75Al25	170	0.48	11.7
Cu07Ni68Al25	178	0.54	12.1
Cu38Ni37Al25	136	0.34	10.3
Cu68Ni07Al25	78	0.40	22.5
Cu75Al25	44	0.17	28
Ni75Fe25	69	0.28	16.3
Cu07Ni68Fe25	99	0.51	20.3
Cu38Ni37Fe25	59	0.33	29
Cu68Ni07Fe25	31	0.19	34
Cu75Fe25	30	0.16	48

Catalysis tests

Processes for the decrease of oxygen content of biomass by hydrodeoxygenation are limited by the drawbacks relative to the use of molecular hydrogen (cost, transport, storage).[39] Alternative hydrogen donors have been proposed, based on catalytic exchange hydrogenation.[40] Several studies have reported data on catalytic hydrogen transfer on Cu-bearing oxides derived from LDHs. In most cases supercritical methanol has played the twin role of solvent and hydrogen donor.[5b,e,41] Tests in methanol at a lower temperature (200 °C) have also shown that it is possible to avoid supercritical conditions, not easily implementable in industrial organosolv processes.[42] The choice of methanol is interesting due to its large availability and the easier separation of gaseous CO and CO_2, coproducts of the hydrogen transfer reaction. However, methanol has a relevant toxicity and is generally not produced from renewable resources. From these points of view, ethanol is more attractive, as largely produced by biomass fermentation and allowed for human use. It is also a more effective hydrogen donor than methanol and has already been proposed for lignin depolymerisation in supercritical conditions.[43]

In the present work, the catalysts obtained from the CuNiAl-LDH and CuNiFe-LDH precursors have been tested in the conversion of 4-benzyloxy-3-methoxybenzaldehyde (BMBA) in subcritical ethanol. Reactions have been conducted at 160 and 200 °C, near the lowest and highest temperature levels commonly used in ethanol organosolv pre-treatment of lignocellulosic biomass.[44] The phenolic ether bond and the carbonyl group of BMBA allowed monitoring of the reactivity of the functional groups most involved in lignin hydrodeoxygenation and depolymerisation. The main products observed in the reaction and their formation pathways are summarized in Scheme 1. Benzyloxymethoxybenzyl alcohol (BMBAlc) and acetaldehyde were formed from BMBA and ethanol by the MPV mechanism of hydrogen cross-exchange between alcohol and aldehyde groups.[4b,40] Acetaldehyde was also formed by direct dehydrogenation of ethanol and the hydrogen species formed were active in hydrogenation reactions beyond the MPV transfer.

Hydrogenolysis of the α-O-4 bond of BMBA led to the formation of vanillin, which was converted to vanillic alcohol by MPV transfer. Hydrogenation of the C–O bond of BMBAlc and

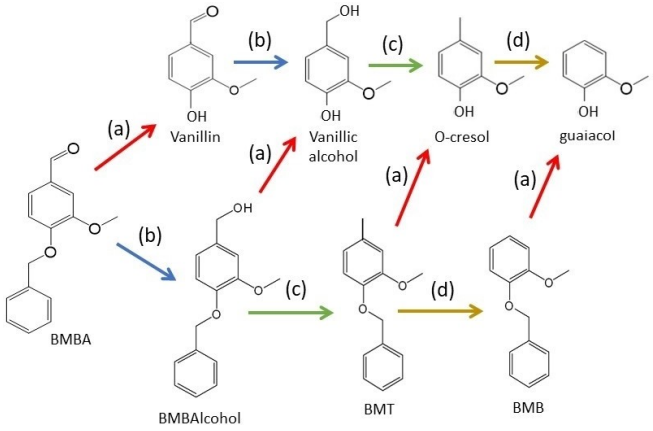

Scheme 1. Cascade of α-O-4 hydrogenolysis (a), MPV (b), C–O hydrogenation (c), C–C hydrogenation (d) reactions of BMBA.

vanillic alcohol formed benzyloxymethoxytoluene (BMT) and o-cresol. Their C–C bonds were further hydrogenated to form benzyloxymethoxybenzene (BMB) and guaiacol.

The activity of the catalysts was significantly dependent on their composition. Conversion, carbon balance and selectivity of the main products observed after 2 h reaction at 160 °C are reported in Table S1. To better follow the effect of the catalyst on the complex cascade of hydrogenation reactions, the results can be presented by type of reaction, namely MPV transfer, α-O-4 hydrogenolysis, C–O hydrogenation and C–C hydrogenation. The sum of yields for the products issued by each type of reaction is presented in Figure 6. The presence of consecutive reactions obviously led to a sum of yields higher than the value of the conversion. As an example, a product like o-cresol, which is the result of consecutive MPV transfer, α-O-4 hydrogenolysis, and C–O hydrogenation, contributes to the yield of each of the three types of reactions considered.

The conversion of BMBA was quite low on the Cu-free catalysts (32% on Ni75Al25 and 23% on Ni75Fe25) and rapidly rose with the Cu content to a maximum at Cu/(Cu + Ni) = 0.5 (95% on Cu38Ni37Al25 and 98% on Cu38Ni37Fe25). At higher Cu content, the conversion slightly decreased in the Al series until 78% at Cu75Al25 but remained almost constant in the Fe series. The mass balance, higher than 95% for all tests with low conversion, was significantly lower in all tests with high conversion, reaching 88% on Cu38Ni37Al25 and 78% on the catalysts of the CuNiFe series with Cu/(Cu + Ni) ≥ 0.5. The observed deficits of carbon balance may be attributed to non-analysed products of consecutive reactions, likely light products of α-O-4 hydrogenation and deeper hydrogenation.

The yield of MPV hydrogen transfer was higher than 90% of conversion on all catalysts with nearly quantitative carbon balance. Only a limited fraction of converted BMBA did not undergo MPV transfer and was converted to small amounts of acetals and esters (see Table S1). This was logically expected by assuming that MPV transfer represents the first step of the cascades of BMBA reactions (see Scheme 1].

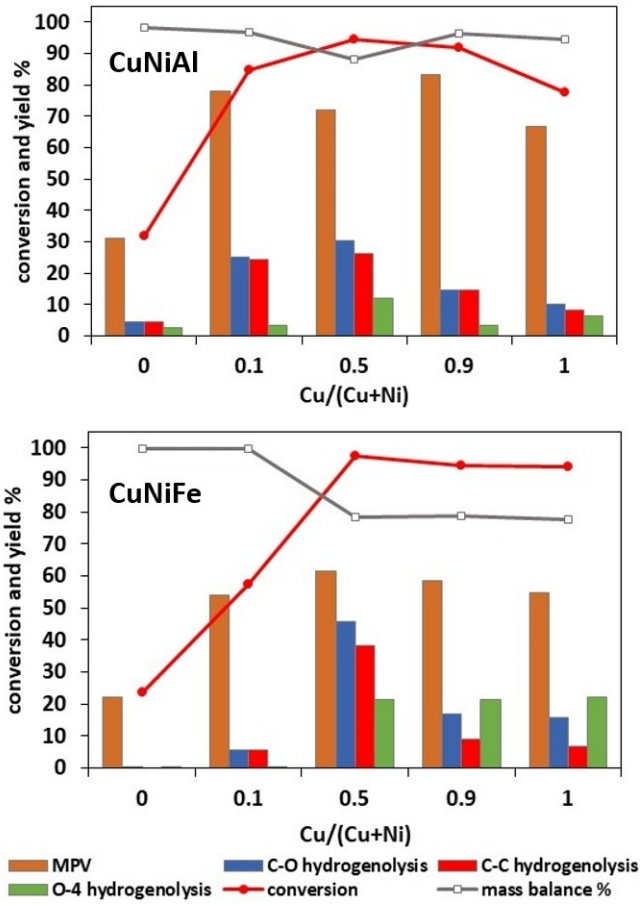

Figure 6. Conversion, carbon balance and yield of BMBA reactions in ethanol at 160 °C for 2 h on catalysts of the Cu–Ni–Al (top) and Cu–Ni–Fe (bottom) series.

The positive effect of Cu on the conversion was also observed on the yield of hydrogenation reactions beyond MPV reaction. Cu-free catalysts were extremely poor in C–C and C–O hydrogenation. The yield of C–O hydrogenation on Cu-free catalysts was very low: 4.6% on Ni75Al25 and just 0.6% on Ni75Fe25, whereas it reached a maximum at 30% on Cu38Ni37Al25 and 46% on Cu38Ni37Fe25. The yield on Ni-free catalysts was somewhat lower than on mixed CuNi catalysts: 10% on Cu75Al25 and 16% on Cu75Fe25, indicating a synergistic effect of Ni on the Cu catalysts. The yield of C–C hydrogenation products was only slightly lower than the yields of C–O hydrogenation, indicating that the hydrodeoxygenation of the alcohol groups formed by MPV transfer was very rapidly followed by the hydrogenation of the aromatic-methyl bonds. However, as already observed for hydrogen transfer from methanol,[42] C–C bonds were less easily hydrogenated in volatile monomers than in dimers. Indeed, o-cresol presented a selectivity higher than guaiacol, while BMT was only observed in traces and BMB was a major product (see Table S1).

The high activity and selectivity of catalytic transfer hydrogenation was correlated with the oxidation states of copper on LDH-derived catalysts.[45] The different activity of Cu- and Ni-bearing catalysts was attributed to easier reducibility of the Cu-

bearing catalysts also in the case of BMBA conversion in methanol.[42] A synergistic effect of Ni on the reducibility of Cu–Ni mixed catalysts was also observed. Cu-bearing catalysts in the Fe series were more active and less selective –due to consecutive reactions- in comparison to the Al series. This effect is especially remarkable when one considers that the catalysts of the CuNiFe series have specific surfaces twofold smaller as those of the CuNiAl series.

The same trends of activity were observed when the reaction temperature was raised to 200 °C. The catalytic activity data in these conditions are reported in Figure 7 and Table S2. The strong effect of the presence of Cu on the activity was confirmed at this temperature. The conversion of BMBA was 68 and 32% for the Cu-free catalysts, respectively in the presence of Al and Fe, while it was higher than 90% for all Cu-bearing catalysts. The carbon balance, near 100% on the Cu-free catalysts, presented a different trend in the CuNiAl and CuNiFe series. In the Al-bearing catalysts, the incorporation of 10% Cu (Cu08Ni67Al25) minimally affected the carbon balance despite an increase of conversion from 68 to 95%. At equivalent Cu and Ni content, the carbon balance presented a minimum at 76%, in correspondence with a maximum conversion at 97%. At higher Cu contents, the conversion slightly decreases and reaches 90% for the Ni-free catalyst, whereas the carbon balance improved up to 90%. In the Fe-bearing catalysts, the introduction of 10% Cu brought to a rise of conversion from 32 to 97% and to a decrease of carbon balance from about 100% to 80%. Further increase in the Cu content brought an increase of conversion up to 100% for Cu68Ni07Fe25 and to a gradual worsening of carbon balance, which reached 67% for the Ni-free Cu75Fe25 catalyst.

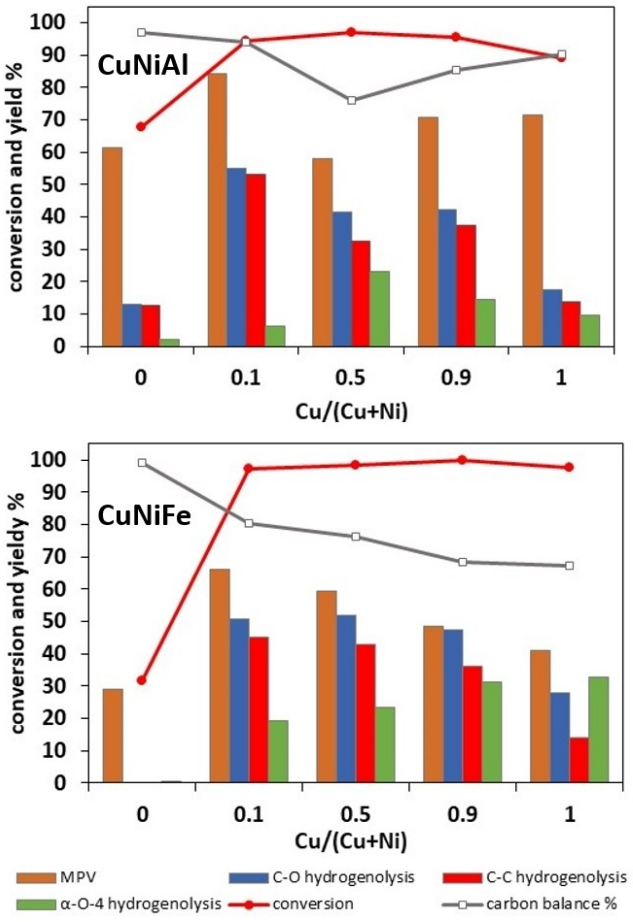

Figure 7. Conversion, carbon balance and yield of BMBA reactions in ethanol at 200 °C for 2 h on catalysts of the Cu–Ni–Al (top) and Cu–Ni–Fe (bottom) series.

MPV hydrogen transfer represented more than 90% of conversion on all catalysts with nearly quantitative carbon balance. The measured MPV yield presented a minimum at Cu/(Cu + Ni) = 0.5 in the Al series and a continuous decrease with Cu content in the Fe series, in correspondence with the worsening of the mass balance. As already observed at 160 °C, the yield of hydrogenation products was very low on Cu-free catalysts: 13% on Ni75Al25 and below the detection threshold for Ni75Fe25. The yield of C–O hydrogenation was at a maximum above 50% for catalysts with 10% Cu/(Cu + Ni) and decreased at higher Cu content.

No products of aromatic dehydrogenation or ring opening were observed. It is interesting to compare these results with the data on hydrogen transfer from ethanol at 340 °C provided by Hensen and co-workers.[43b] In their work, aromatic rings were systematically cleaved in the presence of Mg-bearing Cu catalysts from LDH, while they were preserved on Cu–Al catalysts. It appears that the well-known strong basicity of the mixed oxide obtained from Mg–Al LDH precursor is needed for the opening of the phenolic aromatic rings also in the super-critical conditions of their test.[46] In our experiments, the high density of weaker basic sites provided by Ni is likely at the origin of the observed synergistic effect of nickel on the activity of the Cu catalysts.[47]

In hydrogen transfer processes, the formation of hydrogenation products of the substrate is naturally accompanied by the formation of dehydrogenation products of the hydrogen donor. Separation and reuse of these products can be crucial factors in the assessment of the viability of the process. The use of methanol as hydrogen donor has been proposed because of its low cost and the easy disposal of gaseous CO and CO_2. The use of 2-propanol has been supported by its high effectiveness as a hydrogen donor and by the relative ease of separation of the volatile coproduced acetone. The use of ethanol as a hydrogen donor, in contrast to the advantage of its current production from renewable resources, has to cope with the formation of acetaldehyde, a quite reactive dehydrogenation product.

In our system, the reactivity of acetaldehyde has been monitored by analysis of condensation products. The main product observed was diethoxyethane, the diacetal of acetaldehyde. 1,3-butanediol, butyraldehyde diacetal and 3-hydroxy butyraldehyde were also observed in minor amounts. The amount of diethoxyethane formed in tests at 160 and 200 °C is reported in Figure 8. The trends of formation of the condensation product of acetaldehyde can be compared with the trends of the BMBA reactions (Figures 6 and 7). A fair parallel can be observed between the effects of the nature of

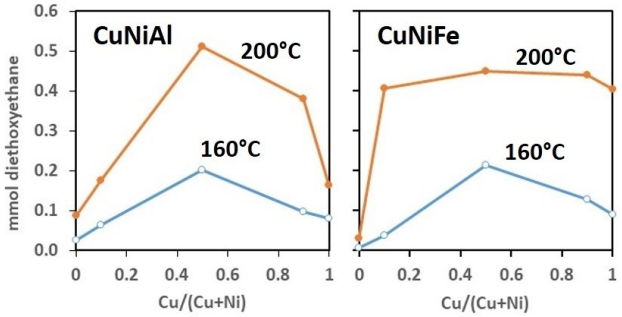

Figure 8. Acetaldehyde diacetal formed on catalysts of the CuNiAl and CuNiFe series in the BMBA reaction at 160 and 200 °C. The lines are a guide for the eye.

the catalyst on the diethoxyethane concentration and the BMBA hydrogenation products. This effect would correspond to a mechanism in which the formation of hydrogen by dehydrogenation of ethanol is the limiting step for hydrogenation reactions beyond the MPV hydrogen transfer. In some way, the best hydrogenation catalysts would be the most effective in ethanol dehydrogenation.

Conclusion

CuNiAl and CuNiFe mixed oxides obtained by activation of LDH are effective catalysts for H-transfer reactions to lignin model molecules in mild reaction conditions and in the absence of added acid or bases. The texture of the catalysts is highly affected by the composition of the precursor LDH. NiO and CuO particles in the calcined material exhibit higher mean crystallite sizes in the CuNiFe than in the CuNiAl system, due to the inhibition of the growth of M(II)O oxides by the matrix of amorphous alumina where they are embedded. On the contrary, the formation of a separate ferrite phase in the CuNiFe system prevents the interaction of the matrix with the crystallites of the M(II)O oxides, leading to easier crystal growth.

The composition of the oxides significantly affected the productivity and selectivity of the reactions. The comparison of catalysts with different composition has allowed identifying a major contribution of Cu to the catalytic activity. However, the most active catalysts have been mixed Cu–Ni oxides, indicating a synergistic role of the high density of relatively weak basic sites provided by Ni. Moreover, Ni introduced in the LDH structures will also provide magnetic properties, useful for the recovery of the catalyst.

The use of Mg-free LDH precursors has contributed to the retention of valuable aromatic rings in the products, preventing the effects of the well-known strong basicity of the mixed oxide obtained from Mg–Al LDH precursor. When comparing the activity of catalysts with different trivalent cations, Fe-bearing catalysts were more active than Al-bearing catalysts, despite their lower surface area. However, the higher activity of Fe-bearing catalysts brought to a worsening of carbon balance and a decrease of product selectivity.

In the presence of the appropriate catalyst, ethanol appears as an effective hydrogen donor for the conversion of lignin materials, not just for MPV hydrogen transfer reactions but also for deeper hydrogenation. Reactions in subcritical ethanol seem appropriate for the breaking of phenylether lignin bonds while retaining valuable aromatic rings.

Experimental Section

Synthesis

Four different LDH precursors were synthesized n Cu–Ni–Al and Cu–Ni–Fe systems. Samples are named by the percent atomic fraction of cations, for instance Cu08Ni67Fe25. Nickel (II) nitrate hexahydrate $\geq$98.5% ($Ni(NO_3)_2.6H_2O$), copper (II) nitrate trihydrate $\geq$99% ($Cu(NO_3)_2.3H_2O$), aluminium nitrate nonahydrate $\geq$98% ($Al(NO_3)_3.9H_2O$), iron (III) nitrate nonahydrate $\geq$99.95% ($Fe(NO_3)_3.9H_2O$), and sodium hydroxide $\geq$97% (NaOH) from Sigma Aldrich and Sodium Carbonate $\geq$99% (Na_2CO_3) from VWR were purchased and used as received without any further purification. Deionized water was used throughout the synthesis experiments. The syntheses were done by co-precipitation at a constant pH of 10 ± 0.1.[48] The cation ratio was $M^{2+}/(M^{2+}+M^{3+}) = 0.75$ (M^{2+} = Ni, Cu and M^{3+} = Fe or Al). Stoichiometric amounts ($M^{2+}/M^{3+} = 3$) of respective nitrate salts ($M(NO_3)_n.xH_2O$) were taken to prepare 0.5 M divalent cation(s) and 0.3 M trivalent cation solutions that were stirred well together to form a homogenous solution. The cationic solution was then added dropwise with a pump into 50 mL of 0.25 M Na_2CO_3 solution at the rate of 0.4 mL/s with constant stirring at 1000 rpm. All syntheses were conducted at 30 °C with controlled addition of alkaline solution NaOH (2 M) by pH-STAT Metrohm 877 Titrino. The resulting slurry was aged for 15 h at 80 °C, unless otherwise stated, under constant stirring at 1000 rpm; centrifuged at 5000 rpm for 10 min; washed three times with deionized water to remove the excess free metal salts and alkali. The samples were dried under vacuum for 3 h and further kept at 80 °C under air flow for 12 h. The catalysts were obtained by calcination of the dried LDH precursors at 600 °C for 6 h with a heating rate of 2 °C/min in air flow.

Characterization

For the structural identification of the materials, powder XRD patterns of the synthesized catalysts were recorded on a Bruker AXS D8 Advance diffractometer with θ-θ Bragg-Brentano setting using nickel-filtered monochromatic CuKα (1.5402 Å) radiation at a 2θ range 4–80 ° with step size 0.02 °. Cell parameters of LDH were calculated by the lines 003, 006 and 110 in rhombohedral setting and by profile refinement from the cell of Yamaoka in monoclinic setting. Phase ratios and cell parameters of the calcined materials were determined by Rietveld treatment. The textural characterization and surface area were studied using conventional adsorption-desorption of N_2 as the adsorbate at 77 K by a multipoint method; conducted using Micrometrics Tristar-3000 automated gas adsorption system with improved vacuum system. Prior to the nitrogen adsorption, the samples were outgassed for 12 h under vacuum at 80 °C for uncalcined samples and 250 °C for calcined samples by Micrometrics VacPrep 061 auto-degassing station. The Brunauer- Emmett-Teller (BET) method was used to evaluate the specific surface area of the catalyst. Pore properties were evaluated by a DFT kernel.[49] The composition of the prepared catalysts was measured by Energy Dispersive X-Ray analysis (EDX) by QUANTA 200F with Detector Oxford Instruments X-Max N SDD/ working

condition at 15 kV/1 μm^3 area, BSE electron in which samples were at vacuum (0.38 torr) at room temperature.

Catalysis

In a typical test, 25 mg of catalyst calcined at 600 °C was introduced in each of six 120 ml autoclaves containing 20 ml of 8 mM solution of 4-benzyloxy-3-methoxybenzaldehyde (BMBA) in anhydrous ethanol. The autoclaves were connected to a Parr 5000 system and deoxygenated by bubbling N_2 in successive cycles of pressurization and depressurization. The closed autoclaves were heated at 5 °C/min and maintained 2 h at 200 °C under stirring at 350 rpm. The liquid products recovered after cooling were identified by GC-MS (Shimadzu GCMS-QP 2010 with a ZB-5HT Inferno low polarity column) and quantified by comparison with standard solutions on a GC-FID equipped with a polyimide Zebron ZB-5HT column. Conversion was calculated from the difference between the concentrations of BMBA at the beginning and the end of the reaction. Yields of products were calculated as molar ratios between aromatic rings of each product and aromatic rings of BMBA reagent. Selectivity of each product was calculated as the ratio of product yield and BMBA conversion.

Conflict of Interest

The authors declare no conflict of interest.

Data Availability Statement

The data that support the findings of this study are available from the corresponding author upon reasonable request.

Keywords: ethanol · hydrogen transfer · lignin · mixed oxides · oxydehydrogenation

[1] a) A. Johansson, O. Aaltonen, P. Ylinen, *Biomass* **1987**, *13*, 45–65; b) M.-F. Li, S. Yang, R.-C. Sun, *Bioresour. Technol.* **2016**, *200*, 971–980.
[2] a) S. Van den Bosch, W. Schutyser, R. Vanholme, T. Driessen, S.-F. Koelewijn, T. Renders, B. De Meester, W. J. J. Huijgen, W. Dehaen, C. M. Courtin, B. Lagrain, W. Boerjan, B. F. Sels, *Energy Environ. Sci.* **2015**, *8*, 1748–1763; b) T. Renders, S. Van den Bosch, S.-F. Koelewijn, W. Schutyser, B. F. Sels, *Energy Environ. Sci.* **2017**, *10*, 1551–1557; c) T. Renders, E. Cooreman, S. Van den Bosch, W. Schutyser, S.-F. Koelewijn, T. Vangeel, A. Deneyer, G. Van den Bossche, C. M. Courtin, B. F. Sels, *Green Chem.* **2018**, *20*, 4607–4619; d) M. M. Abu-Omar, K. Barta, G. T. Beckham, J. S. Luterbacher, J. Ralph, R. Rinaldi, Y. Roman-Leshkov, J. S. M. Samec, B. F. Sels, F. Wang, *Energy Environ. Sci.* **2021**, *14*, 262–292; e) T. Ren, W. Qi, R. Su, Z. He, *ChemCatChem* **2019**, *11*, 639–654.
[3] a) R. Rinaldi, R. Jastrzebski, M. T. Clough, J. Ralph, M. Kennema, P. C. A. Bruijnincx, B. M. Weckhuysen, *Angew. Chem. Int. Ed.* **2016**, *55*, 8164–8215; *Angew. Chem.* **2016**, *128*, 8296–8354; b) Z. Sun, B. Fridrich, A. de Santi, S. Elangovan, K. Barta, *Chem. Rev.* **2018**, *118*, 614–678.
[4] a) P. Ferrini, R. Rinaldi, *Angew. Chem. Int. Ed.* **2014**, *53*, 8634–8639; *Angew. Chem.* **2014**, *126*, 8778–8783; b) A. Lolli, Y. Zhang, F. Basile, F. Cavani, S. Albonetti, in *Chemicals and Fuels from Bio-Based Building Blocks*, Vol. 1 (Eds.: F. Cavani, S. Albonetti, F. Basile, A. Gandini), Wiley-VCH, Weinheim, Germany **2016**, p.353–378; c) W. Sebhat, A. El Roz, P. Fongarland, L. Vilcocq, L. Djakovitch, *Catalysts* **2021**, *11*, 875; d) M. A. Hossain, T. Saelee, S. Tulaphol, M. S. Rahaman, T. K. Phung, T. Maihom, P. Praserthdam, S. Praserthdam, D. J. Yelle, N. Sathitsuksanoh, *ChemCatChem* **2022**, *14*, e202200549.
[5] a) G. S. Macala, T. D. Matson, C. L. Johnson, R. S. Lewis, A. V. Iretskii, P. C. Ford, *ChemSusChem* **2009**, *2*, 215–217; b) K. Barta, T. D. Matson, M. L. Fettig, S. L. Scott, A. V. Iretskii, P. C. Ford, *Green Chem.* **2010**, *12*, 1640–1647; c) T. D. Matson, K. Barta, A. V. Iretskii, P. C. Ford, *J. Am. Chem. Soc.* **2011**, *133*, 14090–14097; d) K. Barta, P. C. Ford, *Acc. Chem. Res.* **2014**, *47*, 1503–1512; e) C. M. Bernt, H. Manesewan, M. Chui, M. Boscolo, P. C. Ford, *ACS Sustainable Chem. Eng.* **2018**, *6*, 2510–2516; f) Z. Sun, G. Bottari, A. Afanasenko, M. C. A. Stuart, P. J. Deuss, B. Fridrich, K. Barta, *Nat. Catal.* **2018**, *1*, 82–92; g) Z. Sun, D. Buwalda, K. Barta, *RSC Adv.* **2019**, *9*, 23727–23734.
[6] a) B. F. Sels, D. E. De Vos, P. A. Jacobs, *Catal. Rev.* **2001**, *43*, 443–488; b) G. Centi, S. Perathoner, *Microporous Mesoporous Mater.* **2008**, *107*, 3–15.
[7] D. Shannon, *Johnson Matthey Technol. Rev.* **2017**, *61*, 172–182.
[8] a) M. J. L. Ginés, N. Amadeo, M. Laborde, C. R. Apesteguia, *Appl. Catal. A* **1995**, *131*, 283–296; b) D. Li, Y. Cai, Y. Ding, R. Li, M. Lu, L. Jiang, *Int. J. Hydrogen Energy* **2015**, *40*, 10016–10025; c) I. Atake, K. Nishida, D. Li, T. Shishido, Y. Oumi, T. Sano, K. Takehira, *J. Mol. Catal. A* **2007**, *275*, 130–138; d) C. Lucarelli, C. Molinari, R. Faure, G. Fornasari, D. Gary, N. Schiaroli, *Appl. Clay Sci.* **2018**, *155*, 103–110.
[9] a) S. R. Segal, K. B. Anderson, K. A. Carrado, C. L. Marshall, *Appl. Catal. A* **2002**, *231*, 215–226; b) S. R. Segal, K. A. Carrado, C. L. Marshall, K. B. Anderson, *Appl. Catal. A* **2003**, *248*, 33–45; c) S. Velu, K. Suzuki, M. Okazaki, M. P. Kapoor, T. Osaki, F. Ohashi, *J. Catal.* **2000**, *194*, 373–384.
[10] a) V. Rives, A. Dubey, S. Kannan, *Phys. Chem. Chem. Phys.* **2001**, *3*, 4826–4836; b) A. Dubey, V. Rives, S. Kannan, *J. Mol. Catal. A* **2002**, *181*, 151–160.
[11] a) R. H. Höppener, E. B. M. Doesburg, J. J. F. Scholten, *Appl. Catal.* **1986**, *25*, 109–119; b) M. Behrens, I. Kasatkin, S. Kühl, G. Weinberg, *Chem. Mater.* **2010**, *22*, 386–397; c) E. M. Fuentes, A. da Costa Faro Jr, T. de Freitas Silva, J. M. Assaf, M. C. Rangel, *Catal. Today* **2011**, *171*, 290–296.
[12] a) F. Cavani, F. Trifirò, A. Vaccari, *Catal. Today* **1991**, *11*, 173–301; b) P. S. Braterman, Z. P. Xu, F. Yarberry in *Layered Double Hydroxides (LDHs), Handbook of Layered Materials* (Eds.: S. M. Auerbach, K. A. Carrado, P. K. Dutta), Marcel Dekker, New York, **2004**, pp. 373–474; c) *Layered Double Hydroxides Present and Future* (Ed.: V. Rives), Nova Science, New York **2001**, 499 pp.
[13] a) G. Fornasari, S. Gusi, F. Trifirò, A. Vaccari, *Ind. Eng. Chem. Res.* **1987**, *26*, 1500–1505; b) A. Alejandre, F. Medina, P. Salagre, X. Correig, J. E. Sueiras, *Chem. Mater.* **1999**, *11*, 939–948.
[14] a) C. Busetto, G. Del Piero, G. Manara, F. Trifirò, A. Vaccari, *J. Catal.* **1984**, *85*, 260–266; b) Y. Lwin, A. B. Mohamad, Z. Yaakob, W. R. W. Daud, *React. Kinet. Catal. Lett.* **2000**, *70*, 303–310; c) Y. Lwin, M. A. Yarmo, Z. Yaakob, A. B. Mohamad, W. R. W, *Mat. Res. Bull.* **2001**, *36*, 193–198; d) A. Alejandre, F. Medina, X. Rodriguez, P. Salagre, Y. Cesteros, J. E. Sueiras, *Appl. Catal. B* **2001**, *30*, 195–207.
[15] S. Tumiati, G. Godard, N. Masciocchi, S. Martini, D. Monticelli, *Eur. J. Mineral.* **2008**, *20*, 73–94.
[16] a) I. Y. Park, K. Kuroda, C. Kato, *Solid State Ionics* **1990**, *42*, 197–203; b) S. Britto, P. V. Kamath, *J. Solid State Chem.* **2009**, *182*,1193–1199; c) M. Intissar, A. Seron, F. Giovannelli, C. Autret, M. Motelica-Heino, F. Delorme, *J. Mater. Sci.* **2015**, *50*, 1427–1434.
[17] S. Consani, T. B. Zunic, A. M. Cardinale, W. Sgroi, G. Giuli, C. Carbone, *Materials.* **2018**, *11*, 130.
[18] T. Yamaoka, M. Abe, M. Tsuji, *Mat. Res. Bull.* **1989**, *24*, 1183–1199.
[19] a) J. Carpentier, S. Siffert, J. F. Lamonier, H. Laversin, A. Aboukaïs, *J. Porous Mater.* **2007**, *14*, 103–110; b) M. Laipan, H. Fu, R. Zhu, L. Sun, J. Zhu, H. He, *Sci. Rep.* **2017**, *77*, 7277; c) W. T. Reichle, *Solid State Ionics* **1986**, *22*, 135–141; R. P. J. Grosso, S. L. Suib, R. S. Weber, P. F. Schubert, *Chem. Mater.* **1992**, *4*, 922–928.
[20] W. Shi, J. Hu, Z.-M. Ni, Y. Li, J. Liu, *Acta Phys.-Chim. Sin.* **2012**, *28*, 1869–1876.
[21] a) L. M. Rossi, N. J. S. Costa, F. P. Silva, R. Wojcieszak, *Green Chem.* **2014**, *16*, 2906–2933; b) J. Huang, C. Zhao, F. Lu, *Polymer* **2018**, *10*, 1077.
[22] J. He, S. Yang, A. Riisager, *Catal. Sci. Technol.* **2018**, *8*, 790–797.
[23] R. Rinaldi, F. Schüth, *Energy Environ. Sci.* **2009**, *2*, 610–626.
[24] a) J. R. H. Ross, in *Surface and Defect Properties of Solids*, Vol. 4 (Eds. M. W. Roberts, J. M. Thomas), The Chemical Society, London, UK, **1975**, pp. 34–67; b) J. R. H. Ross, M. C. F. Steel, A. Zeini-Isfahani, *J. Catal.* **1978**, *52*, 280–290; c) F. Basile, G. Fornasari, E. Poluzzi, A. Vaccari, *Appl. Clay Sci.* **1998**, *13*, 329–345.
[25] R. Unnikrishnan, S. Narayanan, *J. Mol. Catal. A* **1999**, *144*. 173–179.
[26] Q. Wang, X. Wang, B. Tian, *Water Sci. Technol.* **2018**, *77*, 2772.

[27] a) O. Lebedeva, D. Tichit, B. Coq, *Appl. Catal. A* **1999**, *183*, 61–71; b) A. Monzon, E. Romeo, C. Royo, R. Trujillano, F. M. Labajos, V. Rives, *Appl. Catal. A* **1999**, *185*, 53–63.
[28] R. Claydon, J. Wood, *Energy Fuels* **2019**, *33*, 10820–10832.
[29] D. Tyndall, S. Jaskaniec, B. Shortall, A. Roy, L. Gannon, K. O'Neill, M. P. Browne, J. Coelho, C. McGuinness, G. S. Duesberg, V. Nicolosi, *NPJ 2D Mater. Appl.* **2021**, *5*, 73.
[30] a) J. W. Boclair, P. S. Braterman, *Chem. Mater.* **1999**, *11*, 298–302; b) J. W. Boclair, P. S. Braterman, J. Jiang, S. Lou, F. Yarberry, *Chem. Mater.* **1999**, *11*, 303–307; c) A. V. Rhada, P. Vishnu Kamath, *Bull. Mater. Sci.* **2003**, *26*, 661–666; d) C. Ruby, A. Géhin, M. Abdelmoula, J.-M. R. Génin, J.-P. Jolivet, *Solid State Sci.* **2003**, *5*, 1055–1062; e) C. Ruby, R. Aïssa, A. Géhin, J. Cortot, M. Abdelmoula, J.-M. Génin, *C. R. Geosci.* **2006**, *338*, 420–432.
[31] B. Grégoire, C. Ruby, C. Carteret, *Dalton Trans.* **2013**, *42*, 15687–15698.
[32] R. J. M. J. Vogels, J. T. Kloprogge, J. W. Geus, *J. Colloid Interface Sci.* **2005**, *285*, 86–93.
[33] R. Trujillano, M. J. Holgado, J. L. González, V. Rives, *Solid State Sci.* **2005**, *7*, 931–935.
[34] Y. Yang, X. Zhao, Y. Zhu, F. Zhang, *Chem. Mater.* **2012**, *24*, 81–87.
[35] F. Trifirò, A. Vaccari, O. Clause, *Catal. Today* **1994**, *21*, 185–195.
[36] a) M. Jobbagy, G. J. de A. A. Soler-Illia, A. E. Regazzoni, M. A. Bles, *Chem. Mater.* **1998**, *10*, 1632–1637; b) V. Rives, S. Kannan, *J. Mater. Chem.* **2000**, *10*, 489–495.
[37] a) R. J. Hill, J. R. Craig, G. V. Gibbs, *Phys. Chem. Miner.* **1979**, *4*, 317–339; A. M. Balagurov, I. A. Bobrikov, M. S. Maschenko, D. Sangaa, V. G. Simkin, *Crystallogr. Rep.* **2013**, *58*, 710–717.
[38] N. E. Thornburg, M. B. Pecha, D. G. Brandner, M. L. Reed, J. V. Vermaas, W. E. Michener, R. Katahira, T. B. Vinzant, T. D. Foust, B. S. Donohoe, Y. Román-Leshkov, P. N. Ciesielski, G. Beckham, *ChemSusChem* **2020**, *13*, 4495–4509.
[39] A. J. J. Straathof, A. Bampouli, *Biofuels Bioprod. Biorefin.* **2017**, *11*, 798.
[40] M. J. Gilkey, B. Xu, *ACS Catal.* **2016**, *6*, 1420–1436.
[41] a) C. M. Bernt, G. Bottari, J. A. Barrett, S. L. Scott, K. Barta, P. C. Ford, *Catal. Sci. Technol.* **2016**, *6*, 2984–2994; b) C. Espro, B. Gumina, T. Szumelda, E. Paone, F. Mauriello, *Catalysts* **2018**, *8*, 313.
[42] I. Z. Awan, G. Beltrami, D. Bonincontro, O. Gimello, T. Cacciaguerra, N. Tanchoux, A. Martucci, S. Albonetti, F. Cavani, F. Di Renzo, *Appl. Catal. A* **2021**, *609*, 117929.
[43] a) X. Huang, T. I. Kornyi, M. D. Boot, E. J. M. Hensen, *ChemSusChem* **2014**, *7*, 2276–2288; b) X. Huang, C. Atay, T. I. Korányi, M. D. Boot, E. J. M. Hensen, *ACS Catal.* **2015**, *5*, 7359–7370.
[44] N. Park, H.-Y. Kim, B.-W. Koo, Y. Yeo, I.-G. Choi, *Bioresour. Technol.* **2010**, *101*, 7046–7053.
[45] a) J. Zhang, J. Chen, *ACS Sustainable Chem. Eng.* **2017**, *5*, 5982–2993; b) Y. Ren, Y. Yang, L. Chen, L. Wang, Y. Shi, P. Yin, W. Wang, M. Shao, X. Zhang, M. Wie, *Appl. Catal. B* **2022**, *314*, 121515.
[46] a) W. T. Reichle, *J. Catal.* **1985**, *94*, 547–557; b) H. Schaper, J. J. Berg-Slot, W. H. J. Stork, *Appl. Catal.* **1989**, *54*, 79–90; c) D. Tichit, M. H. Lhouty, A. Guida, B. H. Chiche, F. Figueras, A. Auroux, D. Bartalini, E. Garrone, *J. Catal.* **1995**, *151*, 50–59.
[47] a) S. Casenave, H. Martinez, C. Guimon, A. Auroux, V. Hulea, A. Cordoneanu, E. Dumitriu, *Thermochim. Acta* **2001**, *379*, 85–93; b) O. Cairon, E. Dumitriu, C. Guimon, *J. Phys. Chem. C* **2007**, *111*, 8015–8023; c) C. M. Jinesh, C. A. Antonyraj, S. Kannan, *Catal. Today* **2009**, *141*, 176–181; d) L. He, Y. Huang, A. Wang, X. Wang, X. Chen, J. J. Delgado, T. Zhang, *Angew. Chem. Int. Ed.* **2012**, *51*, 6191–6193; *Angew. Chem.* **2012**, *124*, 6295–6298.
[48] I.-C. Marcu, N. Tanchoux, F. Fajula, D. Tichit, *Catal. Lett.* **2013**, *143*, 23–30.
[49] A. Neimark, P. Ravikovitch, *Microporous Mesoporous Mater.* **2001**, *44–45*, 697–707.

Manuscript received: December 19, 2022
Revised manuscript received: February 14, 2023
Accepted manuscript online: February 14, 2023
Version of record online: February 28, 2023